Crystallization Kinetics in Liquid Crystals with Hexagonal Precursor Phases by Calorimetry

Sunkara Padmaja[a], Narayanan Ajita[a], Maddasani Srinivasulu[b], Sriram Ramchandra Girish[b], Venkata Gopala Krishna Murthy Pisipati[c], and Dakshina Murthy Potukuchi[a]

[a] Department of Physics, University College of Engineering, Jawaharlal Nehru Technological University-Kakinada, Kakinada-533003, India
[b] Liquid Crystal Research Centre, ECE Department, Koneru Lakshmaiah College of Engineering, Vaddeswaram, India
[c] Department of Chemistry, Manipal Institute of Technology, Manipal-576104, India

Reprint requests to D. M. P.; E-mail: potukuchidm@yahoo.com

Z. Naturforsch. **65a,** 733 – 744 (2010); received March 28, 2009 / revised September 10, 2009

Design and characterization of Schiff based liquid crystalline nO.m compounds exhibiting hexagonal smectic phases are reported. Crystallization kinetics investigations are carried out in the liquid crystals (LCs) exhibiting hexagonal ordered orthogonal and tilted precursor LC phases by calorimetry. The Avrami theory is referred and results are analyzed. Influence of molecular ordering, structure, and dimensionality of the LC precursor phase on kinetics is studied. Effect of shape and flexibility of the molecule for nucleation and growth processes is investigated. Varying rate of kinetics reflects upon the transit of the system from constant type to independent type of nucleation. The trends in the Avrami parameter b and exponent n suggest sporadic nucleation. Crystal growth is interpreted as heterogeneous permeation of layered domains (or aggregates) formed by needle shaped calamitic molecules. Calorimetric observations at different crystallization temperatures CT and hold time t infer diffusion mediated crystallization.

Key words: Crystallisation; Kinetics; Hexagonal LC Phases; Precursor; Nucleation; Growth; Diffussion.

1. Introduction

Liquid crystals (LCs) possess interesting electro-optic properties and they occupy an important place among display materials [1]. LC systems exhibit dual (disordered fluid and crystalline order) nature and are interesting in the area of soft condensed matter physics [2]. Investigations of the dynamics, scaling laws, and critical fluctuations in the vicinity of a phase transitions involving LC phases aroused interest regarding the fundamental aspects of 1D, 2D or quasi-2D crystal melting. On heating, thermotropic LCs exhibit the crystal (solid) melting transition followed by the appearance of different LC (i. e., smectic followed by nematic) phases. Further heating of LC compound results in the clearing of this LC phase into isotropic liquid. However, when LCs are cooled from high temperature isotropic liquid phase, they condense into LC phases (i. e., nematic phase followed by smectic phases) and finally form a 3D crystalline solid. Crystallization in LCs is studied by heating the crystal (which melts into an LC phase). Crystallization in LCs can also be studied by cooling the high temperature LC phase, which condenses to a 3D-crystal (or solid). The case of crystallization in LCs can be treated as a phase transformation. LC phases are characterized by the long range orientational order. However, the higher ordered smectic LC phases posses layering in addition to one (or two) short range (i. e., within the layers) positional orders. If LCs exhibit the same sequence of phase occurrence in the heating and cooling cycles, they are known as 'enantiotropic'. However, if the meso-phase occurrence happens either in the heating run or in the cooling run only, they are called 'monotropic'.

The growth of LC phase (viz., nematic or smectic) grown by cooling the isotropic liquid is widely reported in literature. But, the growth of a 3D crystal from LC phase is not extensively studied. The growth of crystal from the LC phase [3 – 16] is interesting because the growth is tuned by a wide variety of LC precursor phases with structural diversity. Nevertheless, the recently reported crystallization experiments [5, 12] during the formation of stones in gall bladder

(from the LC phases exhibited by bile) are much more interesting from human physiological point of view. According to Avrami [17], crystallization is treated as a phase transformation [18] involving an evolutionary transit of the system from one phase into the other. The crystallization process takes place in two steps. The initial process involving the origin of embryos (domains of 3D crystal) is known as 'nucleation' step. The second step involving the growth of the domains (with the geometrical features of the on-coming phase) is referred to as 'growth' (or propagation) process. In order to study the crystallization (during the cooling/heating) in LC compounds, the phase that serves as 'harbinger' for the growth of the crystal is considered as the 'precursor phase.' As the precursor LC phase is known to monitor the kinetics of the crystallization process, these phases are also referred as 'kineto-phases'.

The process of crystallization in LCs [3 – 16] is found to be influenced by factors like the rate of cooling, hold (or annealing) time, crystallization temperature, structure of the phase, geometry concerns (of the precursor phases), and shape of the molecule. One of the interesting aspects in smectic LC phases is the hexagonal packing (or pseudo-packing) of molecules in the layers. The growth of smectic phases [19 – 21] with hexagonal ordering, varied dimensionality, and the underlying harmonic scaling are interesting to study. These phases include, viz., quasi-2D phases: smectic-$B_{hexatic}$, smectic-F, and smectic-I phases, orthogonal 3D phases: smectic-B_{cryst}, and tilted 3D phase: smectic-G. The topic of crystallization with hexagonal LC kineto-phases is interesting from fundamental point of view. Initially, the structure and occurrence of an LC phase (with a specific structure) is explained on the basis of the shape of the molecules, viz., through the calamitic [19 – 21] or columnar, sanidic [22], discotic [23], bowlic [24], bow (bent or banana) shaped [25], supra-molecular hydrogen bonded [26], and metal-mesogenic complexes [27] etc. Further more, the increasing end chain length and attaching odd numbered $–CH_2$ units at the end chains are found to induce tilted phases in an LC homologous series [28 – 30].

The body of the data reported [3 – 16] in the field of crystallization in LCs underlines the influence of the shape (calamatic, discotic, bowlic, bent-shape etc.) of the molecule, the flexibility content (length of flexible end chain) of the molecule, and the structural features like tilt etc., of the LC precursor phase for the nucleation and growth processes.

Although crystallization is reported [3 – 16] in LCs (with nematic, cholesteric, smectic-A, smectic-C and smectic-G, and bent precursor phases), the process involving hexagonally ordered precursor LC phases needs to be studied. It is also noticed that the influence of the precursor LC phase need to be resolved distinctly for the nucleation and growth processes.

In the present work, three long chain nO.m compounds, viz., the higher homologues of nO.m compounds, reported to exhibit smectic phases of hexagonal ordering in their orthogonal or tilted versions [28 – 30], are selected. As such, these smectic phases serve as precursor (or kineto) phases towards the study of the crystallization process. The compounds selected are calamitic type of LCs (rod-shaped as shown in Template 1).

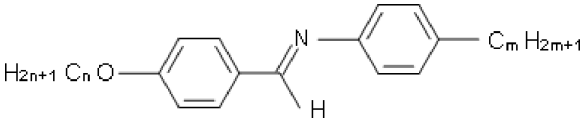

Template 1. General molecular structure of a nO.m molecule.

The paper is organized in four sections. The interesting structural diversity in LCs, importance of crystallization studies, recent reports of crystallization, and the relevance of the Avrami theory are presented in Section 1. For ready reference, the preparation and characterization of the phases and the methodology adopted to study crystallization (by DSC) are briefly presented in Section 2. The meso-phases, transition temperatures, and the enthalpy of transitions are characterized using thermal microscopy by optical polarized light (POM) and differential scanning calorimetry (DSC).

The calorimetric data and it being accessed through the Avrami theory for the interpretation of the crystallization process are presented in Section 3. In Section 4, the trends of the crystallization process with hexagonal smectic kineto-phases in calamitic LCs are presented.

1.1. Avrami Theory

According to Avrami, the crystallization (from phase I to phase II) is considered [17, 18] as a phase transformation which takes place in two steps, viz., nucleation and growth (or propagation). The evolution of a crystal is studied in terms of the rate of the phase transition. However, for the overall process, i. e., for transition from phases I to II, the rate depends on the nucleation and growth. The structural characteristics of

phase II grow in the matrix of phase I. The growth continues until phase I impinges on the growth barriers (like domains or free surfaces).

The fraction of the transformed volume X in a time t is given by

$$X(t) = 1 - \exp[-bt^n]. \quad (1)$$

This equation describes the characteristics of crystallization kinetics with

$3 \leq n \leq 4$ for decreasing rate (depending on t) and
$n > 4$ for increasing rate (depending on t).

b is the rate constant parameter and n is the time exponent. In case of b taking positive values, both parameters (estimated from experimental results) provide information regarding the kinetics of crystallization (see Table 1).

The mechanism for nucleation and growth processes is interpreted depending on the estimated values of n from experiments (calorimetry).

Table 1. Nucleation growth mechanism inferred from the Avrami parameter and exponent.

n-value	Diffusion-Less Nucleation	Diffusion Controlled Growth
0.5		Thickening of plates after their edges get impinged
1.0	Nucleation at start and its continuation at grain boundaries	Growth of isolated needles or plates
1.5		Initial growth of particles nucleates at the start of transformation
2.0	Nucleation at start and its continuation at grain edges	
2.5	Initial growth of particles nucleated at constant rate	
3.0	Nucleation only at the start of transformation	
4.0	i) Nucleation at constant rate ii) Nucleation at increasing rate	

2. Materials

An overview [28 – 30] of the LC phase abundance in nO.m compounds suggest that higher homologues exhibit smectic polymorphism possessing hexagonal packing of molecules. The molecular formula for an nO.m compound was presented in Template 1. The compounds used are the following higher homologues of nO.m series, i. e., for

$n = 16$ and $m = 5$,

$n = 13$ and $m = 16$, and

$n = 10$ and $m = 1$,

viz., 16O.5, 13O.16, and 10O.1, respectively.

For ready reference, the results of thermal microscopy (POM with Olympus Polarizing Microscope and a PC monitored Instec HS1 mK hot stage), the phase transition temperatures T_c and the associated heats of transition and enthalpy ΔH (using Perkin Elmer DSC-7) are presented in Table 2.

The three Schiff based nO.m LCs of interest are reported to exhibit smectic phases with hexagonal ordering [28 – 30]. In the cooling run, they exhibited an orthogonal 3D SmB phase (with hexagonal packing), a 3D tilted SmG phase (with hexagonal packing), and a tilted Quasi-2D SmF phases (with pseudo-hexagonal packing) independently. Further, as the present nO.m compounds possess long end chains, they also provide an opportunity to study the influence of induced disorder for the crystallization process in nO.m compounds [30].

2.1. Methodology

The strategy adopted to study the crystal (solid) growth by DSC involves the isothermal cooling of the LC phase (which serves as precursor phase). DSC is carried out by implementing three successive heating/cooling runs on the LC compound exhibiting the LC precursor phase of interest. In the first run, the heating of the LC compound ensures that it completely melts into its isotropic liquid phase. In the second run, the cooling of the sample ensures the transformation of the isotropic liquid phase into an (or many) LC phase (nematic or smectic). The compound is let to cool down to a specific temperature, i. e. the crystallization temperature CT, into the precursor smectic phase. It was held there and allowed for natural cooling (isothermal) for a finite amount of time viz., the hold time t. During this hold time t the crystal grows. In the third run, heating is again performed on the compound. Any DSC peak that appears in the third run (i. e. heating) is attributed to the melting of the crystal. It is also considered that the hold time t may or may not be sufficient to grow a good amount of volume of the crystal. In the event of insufficient hold time, the DSC thermogram is accompanied by a very small peak or no peak at all. It is also true for the case of insufficient hold time and (or) rapid cooling that the precursor LC phase usually gets super-cooled. In

Table 2. LC phases, transition temperatures (in °C) and ΔH for the compounds 10O.1, 13O.16, and 16O.5.

Compound	Phase Variant	Method		I-N/A/F	N-A	A-B/F	F-G	B/F/G-K
13O.16	FG	TM	Cooling	85.2			81.1	75.0
		DSC	Heating	85.0			[a]	78.1
			ΔH (J/g)	9.5			–	93.3
			Cooling	83.0			80.0[b]	47.0
			ΔH (J/g)	22.1[c]			–	76.2
16O.5	AF	TM	Cooling	84.0		81.8		62.8
		DSC	Heating	90.1		86.3[b]		65.9
			ΔH (J/g)	19.8[c]		–		56.0
			Cooling	84.3		82.3[b]		43.8
			ΔH (J/g)	21.7[c]		–		49.1
10O.1	NAB	TM	Cooling	76.0	74.9	60.5		44.0
		DSC	Heating	76.0	74.9	[a]		69.6
			ΔH (J/g)	3.7	11.3	–		106.2
			Cooling	75.5	74.3	60.3		43.8
			ΔH (J/g)	4.0	11.3	8.0		86.1

[a] Enthalpy for the combined transitions; [b] Peaks are not well resolved; [c] Transitions are not observed.

this latter case, the DSC peak in the third run of heating is due to the melting of meta-stable LC-precursor. However, a comparison of the relevant enthalpy with original values (recorded during the characterization of the LC phases, see Table 2) and the simultaneous optical (microscopic) textural observation are helpful to resolve the issue. The conditions of calorimetry experiments implemented step-wise over an LC compound are given by

1) the heating of the sample to the isotropic phase at a rate of 10 °C/min,

2) holding the sample in the equilibrium isotropic state for a period of about 10 min,

3) fast (and natural) cooling of the sample to a temperature known as crystallization temperature CT into the LC phase (i.e., natural cooling),

4) holding the sample at the CT for a stipulated amount of time t, so that the crystal grows isothermally in this 'hold time',

5) again heating the sample at the rate of 10 °C/min,

6) and recording ΔH associated with the DSC peak (corresponding to crystal melting) appearing in the heating run of Step 5.

2.2. Concept of Precursor Phase and Selection of CT

ΔH corresponding to the crystal melting transformation into the LC phase recorded in the sixth step corresponds to the volume of 3D-crystal grown in Step 4 with in a stipulated hold time. The amount of crystal that is allowed to grow from LC phase for a given hold time t is melted by the heating in Step 5. Thus, this melted part of the crystal is manifested as a DSC endothermic peak with finite ΔH. Since crystal growth in a hold time t at the specific temperature CT is treated as a phase transition, the crystal is argued to grow at the cost of the LC phase formed in Step 3. Now, it is clear that for the crystallization, i. e., a phase transition accompanied by a finite ΔH manifested through a DSC peak in Step 5, the LC phase to which the sample was cooled in Step 3 happens to be the precursor phase.

The amount of crystal grown in the LC precursor phase is reflected through ΔH recorded in Step 6. However, it is also true that ΔH recorded in the sixth step represents the volume of the crystal that has grown in that finite hold time t. Therefore, it is tacitly acceptable that the transformation corresponds to the DSC peak appearing with finite ΔH due to the fifth step of heating reflecting the amount of the volume of crystal grown is preceded with a precursor phase (say SmB in 10O.1). This notional acceptance is based on the preliminary calorimetric data (cooling run) data in Table 2.

A similar strategy is adopted to design the calorimetry experiments for the selection of CT and t for the study of crystallization in 10O.1, 13O.16, and 16O.5 compounds. The CTs are selected such that they fall in the thermal ranges of 50 °C to 58 °C for the 10O.1 compound; 43.8 °C to 55 °C for the 16O.5 compound; and 50 °C to 65 °C for the 13O.16 compound.

2.3. Experiments

The LC sample is initially heated. It was held in the equilibrium isotropic phase for about ten minutes, and then cooled rapidly to the predetermined temperature called 'crystallization temperature' CT. Typical rates observed during the fast (and natural) cooling of

isotropic liquid to the CT are found to be around 50 °C per minute. Then, the sample is held at the predetermined CT for a specified hold time t. The sample is heated at a rate of 10 °C per minute again into the isotropic liquid phase. Now, ΔH corresponding to the melting of the crystal that is grown would appear as a peak. Hence, ΔH reflects the volume of the crystal grown in the LC precursor phase in a finite hold time t. Experiments are repeated using the same sample at different hold times t, such that CT remains constant. The corresponding enthalpy ΔH is recorded.

Thus, calorimetry scans are performed [8 – 10] to study the crystallization process. ΔH is found to increase with increasing hold time t and saturates to an enthalpy value of ΔH_0 i. e., corresponding to a large hold time t in the heating runs. However, fresh samples are used to avoid induction of any trace level impurities of the sample during the DSC scans for each of the predetermined crystallization temperatures CT.

The ΔH associated with the heating of the sample at a predetermined CT and specific hold time t reflecting the volume of crystal grown is found to depend on CT and hold time t. As such, the observed ΔH is normalized with the saturation enthalpy ΔH_0. The ratio $\Delta H/\Delta H_0$ is a characteristic practical measure of the volume fraction of the crystal grown from the LC precursor phase. The evolutionary growth of the crystal grown at different CT and hold time t at the cost of LC precursor phase is studied by the systematic accessing of the data of $\Delta H/\Delta H_0$ recorded at different t to the Avrami equation.

3. Results and Discussion

3.1. Preliminary Characterization of LC Phases

The details of LC phases exhibited by the 10O.1, 13O.16, and 16O.5 compounds, their transition temperatures T_C and the associated heats of transition ΔH observed during POM, i.e., phases identified by comparing with the standard textures [20], and DSC are presented in Table 2. The results of POM are found to agree with those obtained from the DSC. Occurrence of tilted smectic phases (SmG and SmF) in 13O.16 and 16O.5 is argued as due to the orientational disorder [30] induced by long flexible end chains of the molecule.

3.2. Selection of LC Compounds

It is observed that by cooling the high temperature isotropic liquid, the nO.m compounds (viz., 10O.1, 13O.6, and 16O.5) are found to exhibit SmB_{Cryst}, SmG, and SmF phases, respectively, before they solidify into 3D-crystal (solid) phase. It is noticed that the selection of the present nO.m LCs provides an opportunity to study the crystallization with three structurally different LC precursor (kineto) phases, viz.,

i) an orthogonal 3D LC phase (SmB_{cryst} in 10O.1),
ii) a tilted 3D LC phase (SmG with hexagonal tilt distortion in 13O.16), and
iii) a tilted quasi-2D LC phase (SmF with pseudo-hexagonal packing in 16O.5).

The selection of the above compounds also ensures that all the LC precursor (or kineto) phases have a common structural feature of hexagonal packing of molecules. However, the precursor phases in each case differ regarding their arrangement within the smectic layers, i. e., as orthogonal or tilted and the crystalline dimensionality i. e., the additional correlation of hexagons over the layers.

3.3. Detailed Description of Crystallization in LCs

The crystal melting temperatures (B/F/G-K temperatures in Table 2) observed during the heating of the LC compounds are found to bear higher values than those observed during the cooling runs of the sample.

3.3.1 The 10O.1 Compound

DSC (heating) crystallization scans recorded for 10O.1 at a CT of 50 °C as representative are presented in Figure 1. It is observed that the initial heating runs for hold times t of 0 min to 0.4 min are not

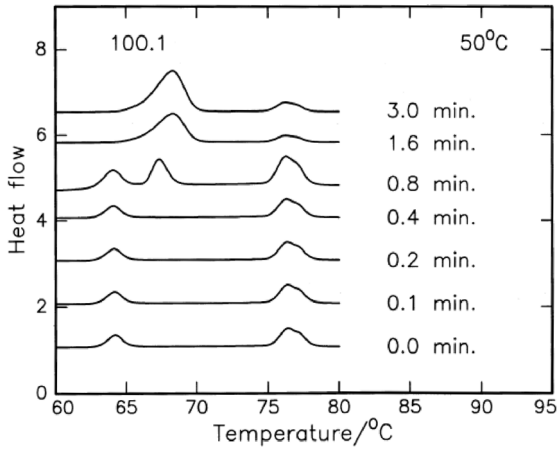

Fig. 1. Crystallization profile for 10O.1 at a CT of 50 °C as representative.

Table 3. ΔH (at specified CT) corresponding to different hold time t for 10O.1.

CT (in °C)	t/min	ΔH (J/g)	t/min	ΔH (J/g)	t^*
50	0.1	0.1	0.2	0.1	1.265145
	0.4	0.2	0.8	10.4	
	1.5	98.6			
52	0.2	0.1	0.4	0.1	2.995020
	0.8	0.12	1.6	43.7	
	3.0	67.5	6.0	97.5	
54	0.2	0.1	0.4	0.11	12.3338
	0.8	0.12	1.6	9.5	
	3.0	9.7	6.0	26.6	
	12.0	67.8	24.0	99.5	
56	0.1	0.01	0.4	0.02	24.22144
	0.8	0.02	1.6	0.02	
	3.0	0.03	6.0	11.8	
	12.0	16.6	24.0	68.4	
	48.0	99.2			
58	0.2	0.01	0.4	0.01	77.49648
	0.8	0.01	1.6	0.02	
	3.0	0.02	6.0	0.02	
	12.0	0.03	24.0	0.03	
	48.0	0.03	96.0	99.3	

accompanied with any appreciable enthalpy, i. e., any DSC peaks in the temperature range less than 64 °C. However, with further increase of the hold time up to 0.8 min a DSC peak, which seems shifted to a temperature of 65 °C, is observed in addition to the other high temperature peaks corresponding to AN and NI transitions. This observed peak bears almost an invariant enthalpy of 8 J/g (see Table 3). As the observed enthalpy remains invariant with hold time, it needs to be resolved whether this peak is due to crystallization or otherwise. It is noticed that the present value of ΔH (equal to 8 J/g) is comparable to the enthalpy relevant to the AB transition at 60.3 °C in the cooling run (Table 2). Simultaneous optical studies of the microscopic focal conic fan texture corresponding to the hold time confirm that this transition is due to the SmB–SmA transition. Thus, the present DSC peak observed up to 0.4 min of hold time in the heating profile for less than 65 °C is considered as due to the melting of metastable SmB into SmA phase. However, for a hold time of 0.8 min, the endotherm exhibited two peaks in the vicinity of 65 °C in addition to the other higher temperature peaks corresponding to the usual AN and NI transitions. Of the two peaks observed around 65 °C, the lower temperature peak is obviously broader and is manifested with an enthalpy of 10.4 J/g. The involvement of large enthalpy infers the case of crystal melting. But the other higher temperature peak is observed to bear an enthalpy of $\sim$ 8 J/g which implies that it corresponds to the SmB–SmA phase transition. The crystallization relevant peak's ΔH in 10O.1 for a CT greater than 0.8 min appears to vary with t to attain the high value of 10.4 J/g. This hold times dependent variation in enthalpy (Table 3) is attributed to the crystal melting transition. An overview of the enthalpy data corresponding to different hold times t seems to pronounce the crystal melting transition with a step-wise increase of ΔH. The crystallization relevant ΔH is observed to remain very small till the hold time reaches a value of 0.8 min. It is also noticed that further increase of hold time results in the merger of these two peaks at 65 – 67 °C to pronounce the crystal melting with a large ΔH. It may be concluded that the conditions for $t > 0.8$ min imposed on the 10O.1 sample at a CT of 50 °C could not further sustain the metastable equilibrium of the SmB phase. Thus, further increase of hold time t is found to result in the large ΔH value of 99 J/g. This value readily coincides with the crystallization ΔH value in Table 2. It may be concluded that for any hold time greater than 0.8 min, the endothermic DSC profile is observed to result in three peaks, viz., the crystal–SmA, SmA–nematic, and nematic–isotropic transitions. Thus, our present interpretation of the DSC profile with increasing hold time t in 10O.1, recorded at a CT of 50 °C as representative, is found to agree with the monotropic (in cooling) SmB occurrence (see Table 2). The $\Delta H(t)$ corresponding to the crystallization in the 10O.1 compound recorded in the heating run seems to follow a sigmoidal variation in accordance with the expectation of Avrami's theory [18].

Simultaneous microscopic textural observations [20] for the formation of characteristic sandy texture for the crystal phase into the LC phase at different CT stands supportive of our interpretation of calorimetric observations.

3.3.2 The 13O.16 Compound

The representative DSC heating profiles recorded at different hold times t for the compound 13O.16 are illustrated for a CT of 53 °C in Figure 2. The endotherms corresponding to different hold times from 0 min to 0.4 min recorded up to a temperature of 90 °C are found to possess only one peak at a temperature $>$ 80 °C. ΔH corresponding to this peak is found to possess an almost constant value of 80 J/g independent of t. This enthalpy value is comparable to that of the recorded across FG transition (see Table 2 in the cool-

Table 4. ΔH (at specified CT) corresponding to different hold time t for 13O.16.

CT (in °C)	t/min	ΔH (J/g)	t/min	ΔH (J/g)	t^*
53	0.1	0.001	0.2	0.002	1.33202
	0.4	9.2	1.0	30.5	
	2.0	88.9	4.0	93.6	
55	0.2	0.001	0.4	0.002	2.261899
	0.8	0.003	1.5	16.3	
	3.0	88.9	6.0	94.3	
57	0.5	0.001	2.0	5.5	5.283612
	4.0	36.1	8.0	93.1	
59	0.5	0.001	1.0	0.002	11.22611
	2.0	0.8	4.0	6.0	
	8.0	27.1	16.0	93.6	
61	0.5	0.001	1.0	0.002	15.57811
	2.0	0.003	4.0	0.004	
	8.0	3.4	16.0	61.1	
	32.0	94.3			
63	0.5	0.001	1.0	0.002	38.64911
	2.0	0.003	4.0	0.004	
	8.0	0.005	16.0	1.5	
	32.0	44.1	60.0	94.2	

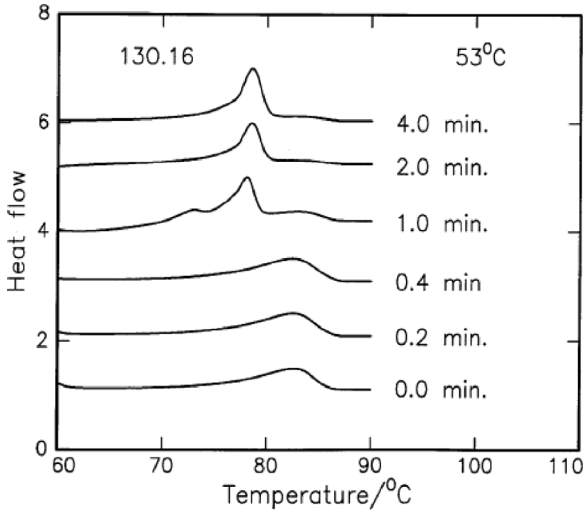

Fig. 2. Crystal melting for 13O.16 at a CT of 53 °C.

ing run). Simultaneous optical observations (broken focal fan textures) also supported that the observed transition for a hold time of 0 min to 0.4 min is of intra smectic type. Therefore, this peak which appears up to 0.4 min of hold time in 13O.16 is attributed to the melting of the meta-stable SmF phase into the isotropic liquid phase. However, the DSC heating profile in 13O.16 for a CT of 53 °C corresponding to a hold time of 1.0 min is found to develop a peak for a temperature less than 80 °C with small ΔH, in addition to the two other high temperature peaks. The two high temperature peaks are interpreted as due to the SmG–SmF and SmF–isotropic phase transitions witnessed during sample heating. A further increase in hold time for 2.0 min is found to accompany with the merger of SmG–SmF and SmF–isotropic transition peaks. The appearance of one DSC peak corresponding to $t \geq 2.0$ min is attributed to the thermal constraints on the system, which could not sustain the meta-stable equilibrium of the SmG phase. This peak for the hold time $t \geq 2.0$ min is interpreted as due to the melting of the crystal grown by cooling the SmG phase into the SmF phase. However, the other higher temperature DSC peak for $t \geq 2.0$ min is due to the melting of the SmF phase into isotropic liquid. Increasing hold time t beyond 2.0 min is found to result in the increase of enthalpy relevant to crystal melting (i.e., saturated to a value of 80 J/g) which can be seen in Table 4. The interpretation of the calorimetric data is found to concur with the values in Table 2 and the optical observations (monotropic, cooling run occurrence of SmG) in 13O.16 compound.

Simultaneous microscopic textural observations [20] of depleting crystal sandy texture and formation of LC texture supports the present interpretation of calorimetric data for the crystallization in the 13O.16 compound.

3.3.3 The 16O.5 Compound

The representative DSC heating profiles for the study of crystallization kinetics in 16O.5 with SmF as precursor phase at a CT of 44 °C are illustrated in Figure 3. The endotherms corresponding to a hold time equal to 0, 0.1, 0.5, and 1.0 min exhibit no crystal melting peak. The two peaks in higher temperature region (for ≥ 80 °C) are attributed to the SmF–SmA and the SmA–isotropic transitions. The DSC peak corresponding to the lowest temperature (≤ 55 °C) is due to the non-equilibrium conditions that prevail between the heating system and the sample. It is observed that once the hold time reaches a value of 2 min, the thermogram is found to accompany with a crystal melting transition into the SmF phase in addition to the SmF–SmA and SmA–isotropic transition peaks. The value of ΔH is found to be small for a hold time ≤ 1.0 min. However, the enthalpy value (Table 5) is found to increase for a hold time ≥ 1.0 min in a step-wise fashion and saturate to a large value of 50 J/g. This large enthalpy value is found to be comparable to the data at T_{FK} in the cooling cycle presented in Table 2. The observed trend of step-wise increment in crystallization

Table 5. ΔH (at specified CT) corresponding to different hold time t for 16O.5.

CT (in °C)	t/min	ΔH (J/g)	t/min	ΔH (J/g)	t^*
44	0.1	0.001	0.5	0.002	2.488011
	1.0	0.003	2.0	27.9	
	4.0	40.4	8.0	50.1	
46	0.1	0.001	0.5	0.002	3.497011
	1.0	0.003	2.0	18.0	
	4.0	35.3	8.0	50.2	
48	0.1	0.001	0.5	0.002	4.104701
	1.0	0.003	2.0	30.3	
	4.0	31.2	8.0	46.1	
	16.0	50.1			
50	0.1	0.001	0.5	0.002	7.791201
	1.0	0.003	2.0	0.004	
	4.0	11.1	8.0	32.2	
	16.0	50.2			
52	0.1	0.001	0.5	0.002	23.43490
	1.0	0.003	2.0	0.004	
	4.0	0.005	8.0	0.53	
	16.0	11.9	32.0	47.8	
	60.0	50.1			

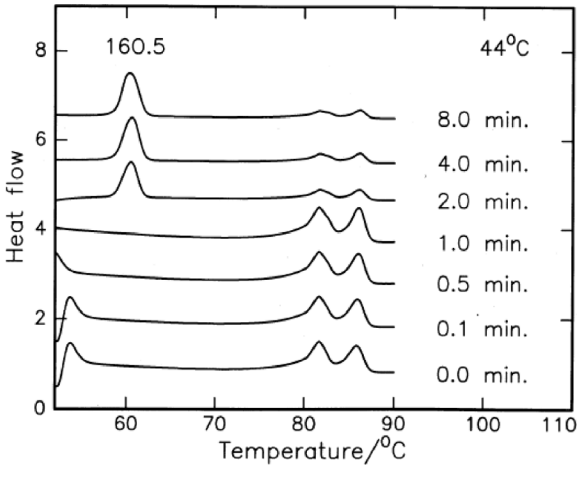

Fig. 3. Crystal melting for 16O.5 at a CT of 44 °C as representative.

relevant ΔH with t (for hold time $t \geq 1.0$ min) is found to agree with Avrami's expectations [18] of sigmoidal growth.

The simultaneous textural (microscopy) observation [20] of the melting of crystalline sandy texture and the formation of LC characteristic texture also confirmed the crystal melting.

3.4. Analysis of Results

The details of CT, t, and ΔH (relevant to the crystallization peak in Step 6) are presented in Tables 3 – 5 for the 10O.1, 13O.16, and 16O.5 compounds, respectively. The data of saturated enthalpy ΔH_0 recorded during the study of crystallization kinetics is also provided. It is observed that the enthalpy ΔH of the crystallization with an LC precursor-phase corresponding to the specified CT appears to follow sigmoidal dependence on hold time t. The observed variation in the enthalpy $\Delta H(t)$ reflects the variation in the volume of the crystal that is grown for a hold time t. ΔH is found to increase nonlinearly with t, and seems to saturate to a value labeled as ΔH_0. However, the ΔH corresponding to each t (at given CT) reflects the fractional increment in volume of the crystal grown. Therefore, the observed enthalpy ΔH at any given CT at different hold times t needs to be normalized over ΔH_0, where ΔH_0 is the enthalpy observed as saturated value of ΔH corresponding to a large hold time. Hence, the value of $\Delta H/\Delta H_0$ represents a realistic measure of the fraction of crystal volume (labeled as X) that is grown for the hold time t of interest. The ΔH_0 values observed for 10O.1, 13O.16, and 16O.5 compounds are 99.51, 94.35, and 50.47 J/g, respectively. It is noticeable that $\Delta H/\Delta H_0$ represents the fractional growth X of 3D crystal from its LC kineto-phase. The crystallization process involves a phase transformation, i. e., the crystal phase grows at the cost of the LC precursor phase. Thus, X is argued to increase at the cost of LC precursor phase (in the given hold time t). Therefore, X is also considered as the fraction of 'transformed volume'. In other words, X represents the fraction of LC volume identified as precursor phase in the third step of the natural cooling run that has transformed into the 3D-crystal at the CT in the given hold time t. The evolution of 3D crystal from LC kineto-phase with hold time t is effectively studied through variation of X with t at any specified CT. An overview of the data of X with t reveals a sigmoidal variation [18] as depicted through the representative Figure 4 . A detailed explanation for the terms in the Avrami equation (1) is helpful to interpret the mechanism for the nucleation and the growth processes in the following way:

b is the Avrami constant which characterizes the embryos, i. e., the domains and their internal geometry that originate transiently during the nucleation step and n is the Avrami exponent that describes the kinetics and growth or the propagation of the domains.

The calorimetric data of crystallization studies is analyzed in the spirit of Avrami's theory. Since X is found to vary (distinctly) with CT and t, the overall crystallization process can be effectively studied by fitting the

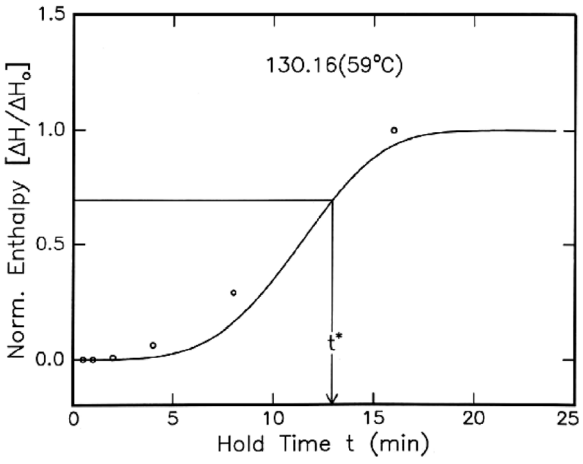

Fig. 4. Growth of crystal (volume fraction) X with time t for 13O.16 for a CT of 59 °C.

calorimetric data to an equation given by

$$X(t) = 1 - \exp[-(t/t^*)^n] \tag{2}$$

and

$$t^* = b^{-1/n},$$

where t^* is a characteristic constant of a specific CT and a set of t adopted during the crystallization process. Hence, t^* is called 'characteristic time'. The value of the characteristic time t^* is estimated by accessing the calorimetric data at each CT to (2). It is implied that t attains a value of t^*, when X equals to 0.632 times of the observed $X_{\max}$. Hence, plots are drawn for X versus t (Fig. 4). The value of t that corresponds to $0.632 \cdot X_{\max}$ is taken as t^*. The estimated t^* values along with the relevant enthalpy ΔH at different CT are presented in Table 6. The estimated t^* values are found to vary with CT. A subtle, but nonlinear relationship appears to exist between t^* and X. In the wake of such fine and discernible relationship between them, the crystal growth seems to be tuned by t^*. As such, the value of n in (2) can be conveniently estimated from the observed dispersal of t^* with X by drawing a logarithmic graph. Hence, a log-log plot is drawn between the characteristic time t^* and X (Fig. 5), viz., between the $\log[-\ln\{1 - \Delta H/\Delta H_0\}]$ and $\log(t/t^*)$. The resulting plot is known as 'Avrami plot'. The corresponding Avrami plots drawn for 10O.1, 13O.16, and 16O.5 are presented in Figure 5. Now, the variation of normalized enthalpy $\Delta H/\Delta H_0$ with t^* given in the logarithmic scale in Figure 5 appears to be linear. As such, the data

Table 6. Spread of characteristic time t^* with CT for the compounds 10O.1, 13O.16, and 16O.5.

Compound (Precursor Phase)	CT (in °C)	t^*	n	b
16O.5 (SmF)	44	2.4880	3.3684	0.04641
	46	3.4970	3.3250	0.01537
	48	4.1047	3.0058	0.01434
	50	7.7912	2.8091	0.00312
	52	23.4349	2.2431	0.00085
13O.16 (SmG)	53	1.3320	4.7075	0.25936
	55	2.2618	4.6865	0.02182
	57	5.2836	4.6555	0.00043
	59	11.2261	3.9667	0.00007
	61	15.5781	3.5596	0.00006
	63	38.6491	2.8254	0.00003
10O.1 (SmB)	50	1.2652	0.6983	0.84855
	52	2.9950	0.7269	0.45048
	54	12.3338	0.4517	0.32151
	56	24.2214	0.3304	0.34891
	58	77.4965	0.1855	0.44615

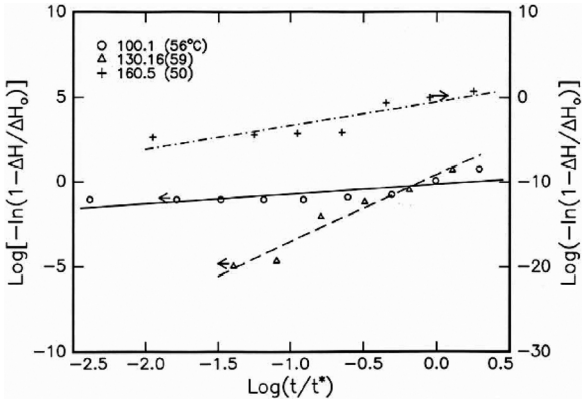

Fig. 5. Avrami plots for the 10O.1, 13O.16 and 16O.5 compounds at specified CT.

is fitted to a linear relation. The value of the Avrami exponent n is estimated from the slope in the Avrami plot determined for the fitted solid line corresponding to different CT. As the observed linearity of the Avrami plot is found to be plausible with (2) the value of b can be estimated from a power law relation given by

$$b = (t^*)^{1/n}. \tag{3}$$

The results of crystallization kinetics in the present LCs regarding the estimated values of the Avrami constant b and the exponent n corresponding to t^* determined at the specified CTs are presented in Table 6. For an overview of crystallization with different precursor phases, the variation of n with CT is presented in Figure 6. It is also observed that n decreases non-

Table 7. Characteristic constant C, decay parameter m, and the variance values for the crystallization in 10O.1, 13O.16, and 16O.5.

Compound	m	C	Variance
10O.1	−0.0711	1.203	0.0542
13O.16	−0.1925	6.185	0.0884
16O.5	−0.1383	3.53	0.0243

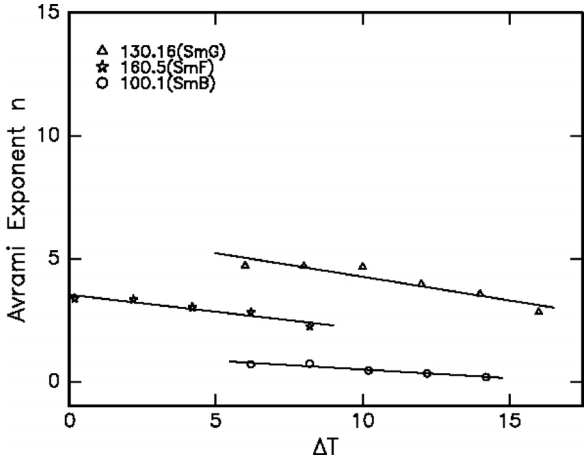

Fig. 6. Temperature variation of Avrami exponent n.

linearly with increasing CT. Therefore, the data of n and CT are fitted to a linear relation given by

$$n(\Delta T) = m\Delta T + C, \tag{4}$$

where $\Delta T = |T_{YK} - T_i|$, and Y = B, G, and F for 10O.1, 13O.16, and 16O.5 LC compounds, respectively. Therefore, T_{YK} is the temperature at which the LC solidifies during the cooling run (Table 2). T_{YK} is 43.8 °C for 10O.1, 43.8 °C for 16O.5, and 47.0 °C for 13O.16.

T_i is the initial temperature for the heating run in Step 5.

The value of C reflects the initial value of n and m reflects the 'decay rate' of n (i. e., decay parameter). The characteristic constants C and m are estimated using the nonlinear least squares method shown as the solid line in Figure 6. The estimated values of C and m are presented in Table 7. The goodness of the fit is demonstrated through the variance values.

It is noticed that a maximum value of m (owing to the negative sign) equal to 0.0711 is associated with crystallization in 10O.1. The decreasing trend of n seems to be three-fold stronger regarding the crystallization with an orthogonal 3D hexagonal SmB precursor phase in comparison to that with SmG or SmF precursor phases. It is noticed that the dimensionality being much higher in precursor SmB phase is tuning the crystallization process in 10O.1. Therefore, it results in the maximum value of n. It is also noticed that the fall in n with CT is rather small in the case of crystallization with tilted quasi-2D SmF or with the 3D tilted SmG LC precursor phases. Although all the three LC compounds of interest with different precursor phases have a common feature of hexagonal packing, the kinetics during the process of crystallization is found to be different. This is argued as due to the underlying LC crystalline dimensionality and the structure of the LC precursor phase. Crystallization for 10O.1 involves the LC SmB precursor phase. The SmB LC phase is an orthogonal phase and possesses 3D correlation of hexagons. This LC phase is frequently referred as SmB_{cryst} phase to underline its 3D structure. It is noticed that a quasi-2D hexatic SmB LC phase with local herring-bone structure (labeled as $SmB_{hexatic}$) differs from SmB_{cryst}. In contrast, the precursor LC phase in 13O.16 is SmG with 3D tilted hexagonal network. Here, the crystallization involves a tilt distortion involving a distortion of bi-axial angle over the smectic layers. In the case of 16O.5, the precursor-phase is SmF with a quasi 2D tilted pseudo-hexagonal network. The relevant crystallization involves a change in tilted LC structure. The variation of n reflecting the geometrical dimensions of the growing domains is expected to be the largest at the crystallization involving the precursor phase with higher dimensionality. As such, the observed three fold higher value of m in 10O.1 is found to be compatible with the expectation. The crystallization with LC tilted precursor phases involves dampening of tilt motion. However, in between the two cases (i. e., SmF in 16O.5 and SmG in 13O.16) of crystallization with tilted LC precursor phases, the case of SmG entails a 3D correlation. Therefore, the fluctuations are expected to grow predominantly at the interface involving the SmG precursor phase in 13O.16 rather than at the interface in 16O.5. In summary, the relative strength of fluctuations as manifested through the decay parameter, i. e., parameter m by accessing the data of n through (4), throws light on the influence of dimensionality of precursor phase on the kinetics of crystallization.

An overview of b values (Table 6) regarding the present investigation of crystallization kinetics reveals that lower values are witnessed at all CTs during the crystallization with SmG precursor phase. The b values with SmF precursor phase are found to be intermediate or lower. But, the crystallization with SmB precursor

phase is found to accompany with the higher values of *b*. The relatively higher values of *b* with SmB precursor phase are attributed to the large volume fraction of crystal grown at the cost of orthogonal 3D (almost) precursor SmB phase.

3.5. Mechanism

The present observation of calorimetry (Fig. 4) concurs with expectations of the Avrami theory. Recently, Joson et al. [13] reported the over all relative suitability of the Avrami theory to the study of crystallization kinetics in LCs with cholesteric precursor phases. The trend of *b* value prevails [18] over the nucleation mechanism. An overview of the present *b* values implies a uniquely decreasing trend with CT. Similar variation of *b* with the CT (or annealing temperature) is reported for the crystallization kinetics in LCs to speak out heterogeneous nucleation [6, 7, 14]. The observed overall lower (but distinctly varying) values of *b* are attributed to the independent type of nucleation mechanism. It is also suggestive for an inhomogeneous permeation of domains [18]. It is found that the *n* values vary from a value greater than 4.7 to a value of 0.34 with the increasing CT. A similar trend of varying Avrami exponent observed in the crystallization kinetics of polymer LCs is argued as due to the varying dimensionality of disclination lines [4]. The observed value of *n* as large as 4.7 (Table 6) is interpreted [18] as the nucleation taking place at constant (or increasing) rate. This unique trend of large variation in *b* is argued as due to the induced orientational disorder [30] by the long flexible end chains of the present LC molecules. However, the observed variation of *n* with the CT is inferred as sporadic type of growth process associated with the crystallization [18]. Recently, the high value of the Avrami exponent is attributed to a sporadic type of nucleation for the crystallization in bent core LCs [11]. It may be recalled that sporadic nucleation is reported with the crystallization in LCs with cholesteric and discotic precursor phases [3, 4]. Nevertheless, the present trend of *n* values suggests that the crystallization process is initiated by nucleation at 'constant rate' [16 – 18]. However, the conspicuous appearance of lower values of *n* at higher CT; and higher values of *n* at lower CT indicate the varied type of nucleation. Similar observations of differing aggregation are reported in aromatic LC esters [14]. It is noticed that the Avrami exponent values of the order of unity are predicted [15] due to the instantaneous nucleation mediated by rod like domain formation. The present case of nucleation is interpreted as a change from the diffusion-less type at lower CT to the diffusion controlled type at higher CT. The lower values of *n* with increasing CT are interpreted as due to the propagation of the domains formed during nucleation by diffusion-less mechanism [16 – 18]. The change of initially observed constant or increasing rate type of nucleation into that of differentiated type of nucleation at higher CT is interpreted as crystallization process mediated through the thickening of plate shaped domains, i. e., the plates with features of smectic layering and/or the aggregation of needle shaped molecules [18]. The domains to be thickened are attributed with plate-like shape due to the fact that the precursor phases in all these cases are layered smectic phases. The attribute given to the aggregates [14] as needle-shaped regions [15] owes to the fact that the precursor LC phases are constituted by rod-shaped (calamitic) molecules. These plates or needles originated as embryos in the nucleation step are further envisaged to impinge at the edges of the embryos during the propagation or growth process.

4. Conclusions

The present crystallization investigations which are studied in the structurally different LC precursor smectic phases formed by the calamitic type of nO.m molecules with long flexible end chains suggest that:

i) Long chain molecules with increased flexible component are capable of forming tilted and hexagonally packed kineto-phases. The increased flexible component induces disorder and indirectly monitors the process of propagation during crystallization.

ii) The Avrami theory can be successfully used to explain the crystallization kinetics in thermotropic liquid crystals.

iii) The crystallization kinetics associated with higher dimensionality LC precursor phases dominates over that involving lower dimensional LC phases.

iv) Hexagonally packed LC precursor phases lead to diffusion controlled crystallization.

v) Although the kineto-phases differ in their structure and dimensionality, the mechanism during the nucleation step of crystallization in all calamitic type of thermotropic LCs is found to be uniquely mediated by the sporadic type. The propagation process is found to involve inhomogeneous permeation of embryos formed during the nucleation step [18].

[1] D. Demus, in: Non Emissive Electro-optic Displays (Ed. A. R. Knetz and F. K. Von Willison), Plenum Press, New York 1976, p. 94; L. M. Blinov and G. Chigrinov, in: Electro-optic Effects in Liquid Crystal Materials, Springer-Verlag, New York 1995; J. W. Goodby, R. Blinc, N. A. Clark, S. T. Lagerwall, S. A. Osipov, S. A. Pikin, T. Sakurai, Y. Yushino, and B. Zeks, in: Ferroelectric Liquid Crystals, Principles, Properties and Applications (Eds. G. W. Taylor), Gordon and Breach, Philadelphia 1991.
[2] N. A. Clark and S. T. Lagerwall, in: Recent Developments in Condensed Matter Physics (Ed. J. T. Devreese, L. F. Lemmens, V. E. Van Doren, and J. Van Royen), Plenum Press, New York 1981, **5**, 309; J. D. Litster, R. J. Birgeneau, and P. E. Pershan, Physics Today **35**, 261 (1982); J. D. Brock, R. J. Birgeneau, J. D. Litster, and A. Aharany, Physics Today **7**, 52 (1989).
[3] F. P. Price and J. H. Wendorff, J. Phys. Chem. **75**, 2849 (1971); ibid.; J. Phys. Chem. **76**, 276 (1972).
[4] S. R. Zhao, A. Schaper, and W. Ruland, Acta Polymerica **44**, 173 (1993).
[5] D. Q.-H. Wang and W. M. C. Cerey, J. Lipid. Res. **37**, 2539 (1996).
[6] Z. He, Y. Zhao, and A. Caille, Liq. Cryst. **23**, 317 (1997).
[7] S. L. Liu, S. Chung, L. Lu, Y. Tori, H. Oikawa, H. Yamaguchi, J. Polymer Science B **36**, 1679 (1998).
[8] P. A. Kumar, M. L. N. Madhu Mohan, and V. G. K. M. Pisipati, Liq. Cryst. **27**, 727 (2000).
[9] M. Srinivasulu, P. V. V. Satyanarayana, P. A. Kumar, and V. G. K. M. Pisipati, Mol. Mater. **14**, 215 (2001); ibid Liq. Cryst. **28**, 1321 (2001); ibid Z. Naturforsch. **56a**, 681 (2001).
[10] P. Swathi, P. A. Kumar, and V. G. K. M. Pisipati, Liq. Cryst. **28**, 1163 (2001); ibid Mol. Mater. Mol. Mater. **14**, 319 (2001).
[11] I. Dierking, Physica B **304**, 51 (2001).
[12] H. Yang, J. Wu, J.-Y. Li, L. Gu, and M.-F. Zhau, World J. Gastroenterology **9**, 1791 (2003).
[13] T. F. Joson, L. T. Danilla, and Z. B. Domingo, Science Diliman **15**, 51 (2003).
[14] Q. Gu, S. Chen, and Y. Yuang, Polymer **45**, 2817 (2004).
[15] E. Perez, B. Pena, and A. Bello, Polym. Bullet. **33**, 451 (1994).
[16] T. Chitravel, M. L. N. Madhumohan, and V. Krishna Kumar, Mol. Cryst. Liq. Cryst. **493**, 17 (2008).
[17] M. Avrami, J. Chem. Phys. **7**, 1103 (1939); ibid J. Chem. Phys. **8**, 212 (1940).
[18] C. N. R. Rao and K. J. Rao, in: Phase Transitions in Solids, McGraw-Hill, New York 1978, p. 91.
[19] P. G. de Gennes and J. Prost, in: The Physics of Liquid Crystals, 2nd Ed., Clarendon, Oxford 1993, p. 277.
[20] G. W. Gray and J. W. Goodby, in: Smectic Liquid Crystals – Textures and Structures, Leonord Hill, London 1984.
[21] S. Chandrasekhar, in: Liquid Crystals (Ed. N. M. Woolfson and J. Ziman), Cambridge University Press, Cambridge 1977, p. 274.
[22] H. Stegemeyer, in: Liquid Crystals (Ed.: H. Baumgerkel, E. U. Franck, and W. Grunbein), Springer, New York 1994, p. 47.
[23] S. Chandrasekhar, B. K. Sadashiva, and K. A. Suresh, Pramana, **9**, 471 (1977).
[24] L. Lam, Mol. Cryst. Liq. Cryst. **155**, 531 (1988).
[25] T. Niori, T. Sekine, J. Watanabe, T. Furukawa, and H. J. Takezoe, Mater. Chem. **6**, 1231 (1996).
[26] T. Kato and J. M. J. Frechet, J. Am. Chem. Soc. **3**, 8533 (1989).
[27] H. Adams, N. A. Bailey, D. W. Bruce, R. Dhillon, D. A. Dunmur, S. E. Hunt, E. Lalinde, A. A. Maggs, R. Orr, P. Styring, M. S. Wragg, and P. E. Maitlis, Polyhedron, **7**, 1861 (1988).
[28] V. G. K. M. Pisipati, Z. Naturforsch. **58a**, 661 (2003).
[29] S. Padmaja, M. Srinivasulu, and V. G. K. M. Pisipati, Z. Naturforsch. **58a**, 73 (2003).
[30] S. Padmaja, M. R. N. Rao, P. V. D. Prasad, and V. G. K. M. Pisipati, Z. Naturforsch. **60a**, 296 (2005).
[31] N. V. S. Rao and V. G. K. M. Pisipati, J. Phys. Chem. **87**, 899 (1983).